Numerical simulation of the effect of strip entry temperature on continuous galvanizing bath management and dross formation

Yu, K. R.; Ilinca, F.; Goodwin, F. E.

Publisher's version / Version de l'éditeur:

2016 AISTech Conference Proceedings, 2016-05

Numerical Simulation of the Effect of Strip Entry Temperature on Continuous Galvanizing Bath Management and Dross Formation

K. R. Yu[1], F. Ilinca[1], F. E. Goodwin[2]

[1] National Research Council of Canada
75 de Mortagne, Boucherville, Québec, Canada. J4B 6Y4
Phone: (450) 641-5072
Email: florin.ilinca@cnrc-nrc.gc.ca; kintakraymond.yu@cnrc-nrc.gc.ca

[2] International Zinc Association
2530 Meridian Parkway, Ste. 115, Durham, NC 27713
Phone: (919) 361-4647
Email: fgoodwin@zinc.org

Keywords: Dross formation, Continuous Galvanizing Bath, Numerical modeling, Strip Entry Temperature

ABSTRACT

Achieving a good and stable thermal field and controlling the content of aluminum and iron in the continuous galvanizing bath operations are of critical importance in achieving automotive quality coated steel products. Due to the prior over-aging heat treatment, the strip entry temperature for advanced high strength steels (AHSS) may be different from the mean bath temperature. Such temperature difference may have significant impacts on the bath thermal field and consequently the dross formation patterns, potentially hampering the quality of the coating surface. In the present study, the effect of the strip entry temperature on galvanizing bath management is examined numerically using a well-validated galvanizing bath model. The impacts are quantified in terms of the bath flow, temperature and compositional characteristics, as well as the dross formation pattern for five different strip entry temperatures from 420 to 500°C. For each case, the Fe dissolution and Al uptake rates are adjusted according to the predictions of the MAP (Modeling Aluminum Pick-up) program from Teck Metals Ltd. It is found that the difference in the strip entry temperature can induce substantial variations in the galvanizing bath temperature field. The results of the present study suggest that a higher strip entry temperature may be potentially beneficial to reduce both the power consumption and the overall dross formation. Certainly, it demands a good local temperature management to prevent excessive dross formation.

INTRODUCTION

Recently, advanced high strength steels (AHSS) have become popular in the automotive industry due to their unique combined light weight and high strength characteristics. These desired properties are obtained from proper addition of alloying elements and carefully controlled heat treatments [1]. The strip entry temperature of AHSS, typical of over-aging treatments, can sometimes be lower than the mean bath temperature. Meanwhile, strip entry temperatures higher than the bath temperature could also occur for extended over-aging time or with inadequate rapid jet cool capacity. Such temperature difference may have significant impacts on the bath thermal field. A local decrease in the bath temperature reduces the solubility of both iron and aluminum in the bath, which in turns promotes the formation of dross particles. It is well-known that dross formation is a major obstacle in the production of high quality galvanizing coating [2]. Therefore, it is needed to better understand the potential impact of the strip entry temperature difference on galvanizing bath management.

Numerical simulation has shown to be a cost effective tool to examine the characteristics of the flow field of the galvanizing bath. A three-dimensional numerical model had previously been developed to determine the flow, temperature and compositional characteristics for various galvanizing bath operations [3]–[6]. The galvanizing bath model had been validated against real-time plant data for a complex transition process from galvanneal (GA) to galvanizing (GI) operations [7]. The simulation results and the plant data are in excellent agreement.

To examine the impact of the strip entry temperature difference, a parametric study is performed. Five different strip entry temperatures from 420 to 500°C are considered. The case of $T_{strip} = 460$°C, which is the same as the typical mean bath temperature, is set as reference in the comparison.

The paper is organized as follows: First, the numerical model for the galvanizing bath is described. The methodology for the numerical experiment is then explained. After, the key characteristics of the temperature field and the solute concentration of the galvanizing bath, as well as those of the dross formation, for the five cases are presented and discussed. The findings are summarized in the conclusion.

NUMERICAL MODEL

Overview of the galvanizing bath model

The configuration of a typical 250 ton galvanizing bath is shown in **Error! Reference source not found.**. The steel strip enters the galvanizing bath through the snout region. It turns around the sink roll and exits the molten zinc bath directed by a set of guide rolls. Aluminum is often added to the zinc bath to improve corrosion resistance [8]. It forms a thin (generally $< 1\ \mu m$) inhibition layer of Fe_2Al_5 on the surface of the strip. Hence, it is needed to add aluminum ingots in order to compensate the consumption, where the inductor provides the required energy for the ingots melting. In the model, the heating rate of the inductor can be adapted to reflect the different ingot loading cycles. Besides the heating from the inductor, the overall heat balance also considers the heat losses through the sidewalls, the top and the bottom surfaces of the bath. Furthermore, operating parameters such as line speed, strip width, and strip temperature can be adjusted.

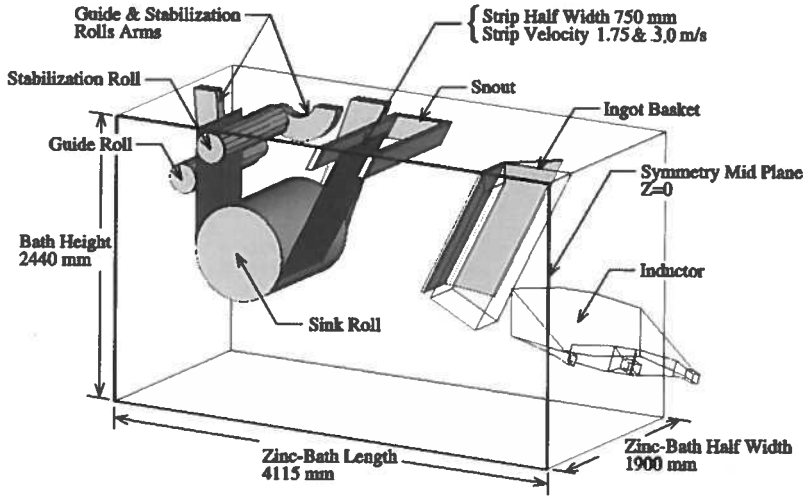

Figure 1: A typical galvanizing bath configuration (half of the bath width shown)

Governing equations and analytical model

The molten liquid Zn-Al alloy is modeled as an incompressible Newtonian fluid. The turbulent bath flow is determined using the standard $k - \varepsilon$ turbulence model in the positivity preserving logarithmic form [9]. The buoyancy effects are considered using the Boussinesq approximation. The mass balance of the solute concentrations of iron Fe and aluminum Al are described by the convection-diffusion equations. The formation of intermetallic dross particles is determined by the solubility limit of the solute components indicated by the phase diagram of the alloy system and depends on the local solute concentrations and the bath temperature [10], [11].

The melting of the ingots is modeled in the energy and mass transport equations using flux boundary conditions at the ingot/bath interface; meanwhile the iron and aluminum dissolution and consumption are implemented as flux boundary conditions respectively on the strip surface in the strip entry region.

It is assumed that the formation/dissolution of dross precipitates occurs instantaneously, and that any new addition of solute components results in the nucleation of dross particles when the total solute concentration exceeds the solubility limit of the specific composition of the bath. Besides, the dross particles are assumed to be sufficiently small that they have negligible influences on the molten Zn flow. Also, no agglomeration of the dross particles occurs during their movements in the bath. The simulations, based on these assumptions, have successfully demonstrated the sensitivity of dross formation to temperature variations.

The governing equations are discretized using finite element method. In particular, the Navier-Stokes and the scalar transport equations are solved using a streamline-upwind Petrov-Galerkin (SUPG) approach [12]. The resulting global system of equations is solved in a partly segregated manner [7].

For further information regarding the galvanizing bath model, the reader is referred to Ilinca et al. [7]. Note that the galvanizing bath configuration considered in the present study does not have the wall heating feature.

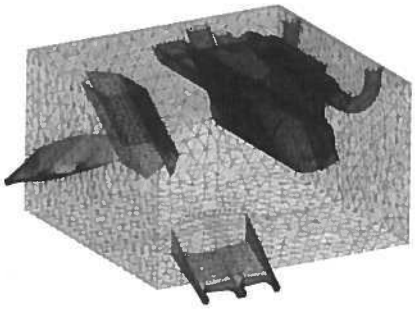

a) Mesh: # of nodes 315831, # of elements 1801085

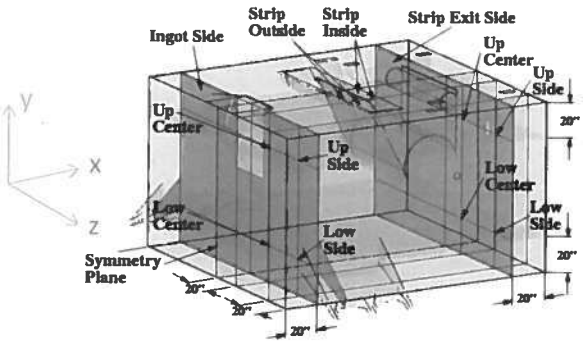

b) Sampling locations for field properties.

Figure 2: Computational domain

Computational domain

The computational domain is discretized using four-node tetrahedral elements with a mesh of 315831 nodes and 1801085 elements, shown in Figure 2a. The system of equations is solved in parallel using a Beowulf cluster.

METHODOLOGY

Simulations are performed for a two-hour operation period for each of the five strip entry temperatures considered: $T_{strip} = \{420°C, 440°C, 460°C, 480°C, 500°C\}$. The case of $T_{strip} = 460°C$, which is the same as the typical galvanizing bath temperature, is selected as reference. The overall temperature distribution, solute concentrations and the dross formation characteristics are examined, as well as those at 12 specifically chosen locations in the bath (**Error! Reference source not found.**Figure 2b). The coordinates of selected locations are listed in Table 1.

Table 1: Sampling locations for field properties

Location	Name	X (in/mm)	Y (in/mm)	Z (in/mm)
Ingot Side	Up-Center	-61 / -1549	-20 / -508	20 / 508
	Up-Side	-61 / -1549	-20 / -508	55 / 1397
	Low-Center	-61 / -1549	-76 / -1930	20 / 508
	Low-Side	-61 / -1549	-76 / -1930	55 / 1397
Strip Exit Side	Up-Center	61 / 1549	-20 / -508	20 / 508
	Up-Side	61 / 1549	-20 / -508	55 / 1397
	Low-Center	61 / 1549	-76 / -1930	20 / 508
	Low-Side	61 / 1549	-76 / -1930	55 / 1397
Snout Region	Inside-Center	0 / 0	0 / 0	0 / 0
	Inside-Extremity	-3 / -76	0 / 0	36 / 914
	Outside-Center	-7 / -196	0 / 0	0 / 0
	Outside-Extremity	-3 / -76	0 / 0	-36 / -914

For the present study, conventional steel is considered. Hence, there is no other alloying metal (e.g. manganese) in the bath. A gradual (or continuous) ingot loading scheme is chosen, as opposed to a periodic ingot loading scheme, to minimize the fluctuations of the concentrations of aluminum. This allows closer examinations of the dross formation characteristics. For the present case, Zn-0.5% Al ingot is considered and the dominant dross species is Fe_2Al_5.

Table 2: Parameters for the inductor operations for the considered strip entry temperatures

T_{strip}(°C)	Flow rate	$T_{increase}$(°C)	Power[1]
420	100%	+15.6	78%
440	100%	+12.5	63%
460	**100%**	**+9.5**	**48%**
480	100%	+6.4	32%
500	100%	+3.5	17%

The difference in the strip entry temperature disturbs the global energy balance of the bath. Prior to the numerical analysis, the parameters for the inductor operations are first adjusted to ensure that the overall mean galvanizing bath temperature is maintained at $T_{bath} = 460°C$ over the two hours operation period. The parameters for the inductor operations for the various strip entry temperatures are listed in Table 2. The overall power input from the inductors and the heat balance of the galvanizing bath for $T_{strip} = 460°C$ are shown in Figure 3 which illustrates that constant overall heat balance is attained.

Besides the overall heat balance, it is well known that the difference in the strip entry temperature also influences the Fe dissolution and the Al uptake rates of the strip [13]. For each strip entry temperature, these rates are adjusted according to the prediction of the well validated MAP (Modeling Aluminum Pick-up) program from Teck Metals Ltd. [14]. The line speed is set at 105m/min, and the strip immersion length is 3.12 m. The bath temperature is considered as constant at 460 °C and the bath Al content is at 0.14 wt %. When the strip entry temperature increases, the predicted Fe dissolution rate decreases; in contrast the Al uptake rate slightly

[1] Note that the inductor in the galvanizing bath model is capable to deliver a temperature increase of 20 °C at full power.

increases. The predictions agree well with the experimental observation that a higher strip entry temperature promotes the formation of the Fe_2Al_5 inhibition layer [15], which prevents the Fe dissolving into the bath.

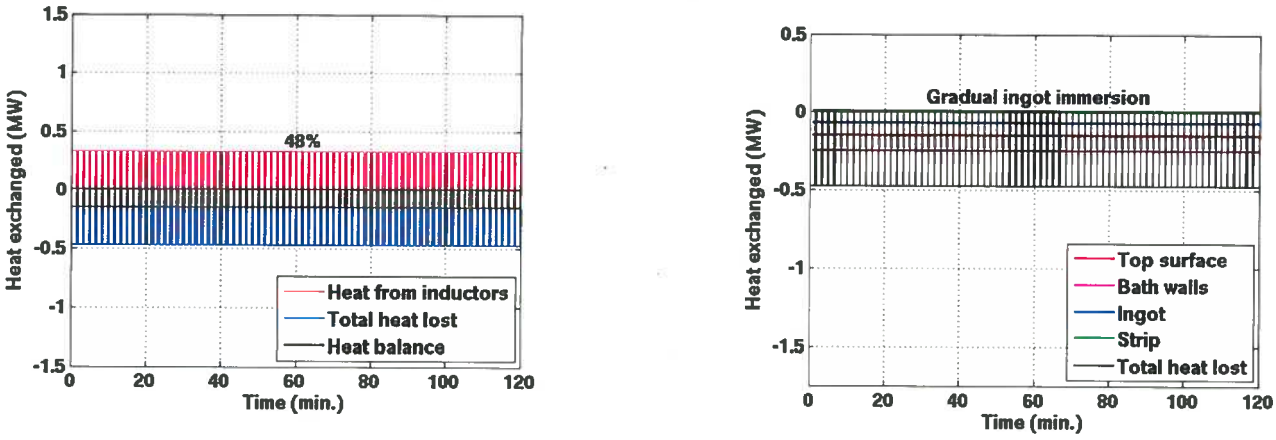

a) Power input from the inductors b) Heat balance

Figure 3: Overall power input and heat balance of the bath for $T_{strip} = 460$°C

RESULTS

Temperature distribution

The overall temperature distributions in the bath for the five strip entry temperatures are shown in Figure 4a-e. The influence of the strip entry temperature can be clearly observed at the snout and sink roll areas. Due to the gradual ingot loading scheme, the ingot loading region appears to be cool for all cases. The areas above the ingot loading region exhibit an opposite trend with respect to the strip entry temperature. This region receives the flows directly from the inductors. Recall that for a low strip entry temperature, the inductors are required to operate at a higher power to ensure the global energy balance, which results in a higher temperature in this area. The reverse is observed for a high strip entry temperature.

The local temperature evolutions at the ingot, the strip exit and the snout regions are shown in Figure 5a-c for the reference case of $T_{strip} = 460$°C. Generally, the local temperatures remain close to the mean bath temperature. At the ingot loading region (Figure 5a), the area above the ingot loading area is about 1°C warmer than the mean bath temperature; whereas the area below is about 1°C cooler. The temperature differences are much smaller at the strip exit (Figure 5b) and the snout region (Figure 5c).

At $T_{strip} = 420$°C, the temperature above the ingot loading area reaches 2°C higher than the mean bath temperature (Figure 6a). Other than the expected much colder center areas at the snout and the strip exit regions (Figure 6b-c), the other local temperatures at these two regions remain close to the mean bath temperature. The local temperature profiles at $T_{strip} = 440$°C are similar to those at $T_{strip} = 420$°C with smaller variations. Therefore, it is not shown here.

In contrast, the local temperatures at the ingot area at $T_{strip} = 500$°C all remain close to the mean bath temperature (Figure 7a). The same is true for the strip exit region (Figure 7b). At the snout region, much higher temperature is observed at the center area as expected (Figure 7c). Likewise, the local temperature profiles at $T_{strip} = 480$°C are similar to those at $T_{strip} = 500$°C with smaller differences; hence, not shown.

Bath Al and Fe concentration

The evolution of the overall mean aluminum and iron concentrations is shown in Figure 8. The mean aluminum concentration increases continuously which reflects the chosen ingot melting scheme correctly. The same rate is observed for all cases.

The mean iron concentration also increases continuously, but with subtle differences. This becomes more evident at the later period, in particular after 80 minutes of simulation time. A slightly higher mean Fe concentration is observed for a lower strip entry temperature. As the strip entry temperature increases, the mean Fe concentration becomes smaller. These correspond well with the imposed boundary condition due to the Fe dissolution rate, which is predicted to decrease when the strip entry temperature increases.

The local aluminum and iron concentration characteristics for the different strip entry temperatures behave similar to the overall mean values, with the addition of the influences of local flow fields. Therefore, they are not shown here.

The continuously increasing mean aluminum and iron concentrations lead to constantly increasing dross formation, which are presented next.

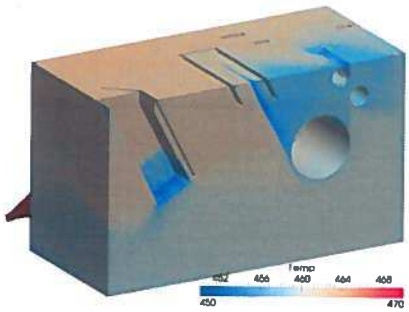

a) Temperature distribution for $T_{strip} = 420°C$

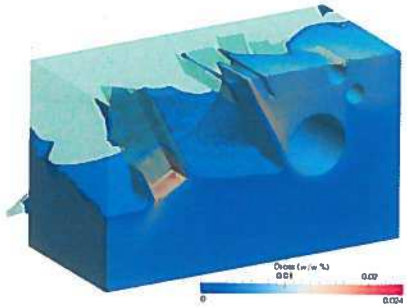

f) Dross formation for $T_{strip} = 420°C$

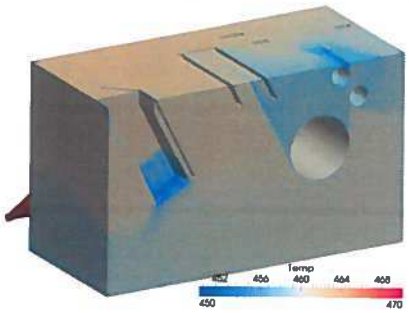

b) Temperature distribution for $T_{strip} = 440°C$

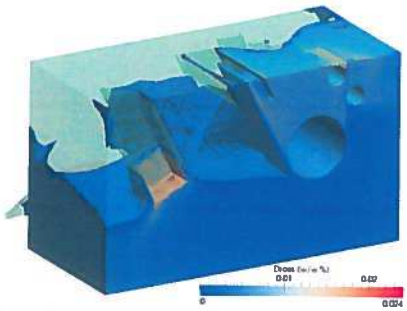

g) Dross formation for $T_{strip} = 440°C$

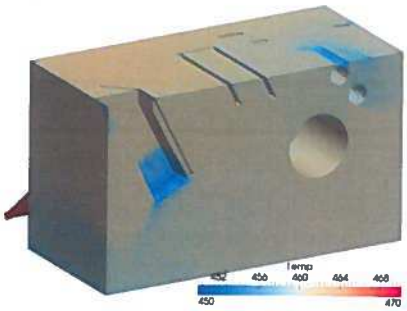

c) Temperature distribution for $T_{strip} = 460°C$

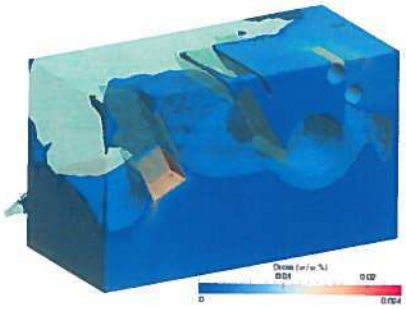

h) Dross formation for $T_{strip} = 460°C$

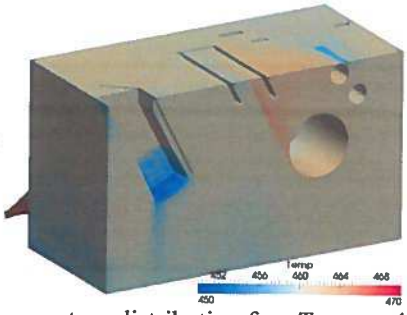

d) Temperature distribution for $T_{strip} = 480°C$

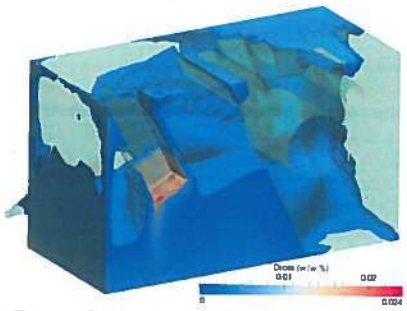

i) Dross formation for $T_{strip} = 480°C$

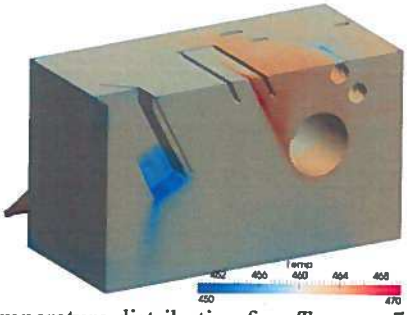

e) Temperature distribution for $T_{strip} = 500°C$

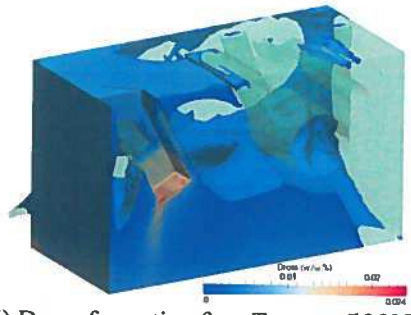

j) Dross formation for $T_{strip} = 500°C$

Figure 4: Overall temperature distribution and dross formation with respect to strip entry temperature

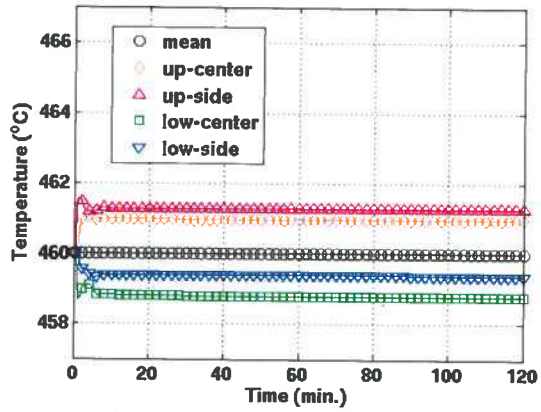

a) Temperature at the ingot region

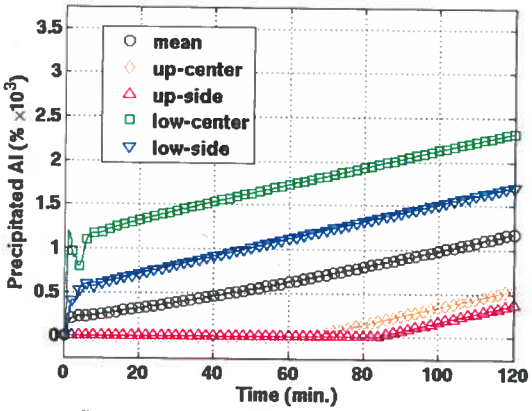

d) Dross formation at the ingot region

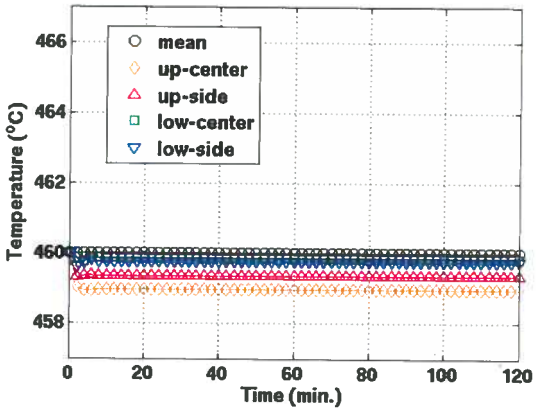

b) Temperature at the strip exit region

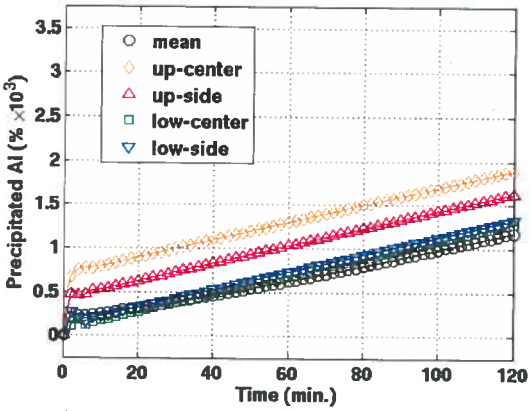

e) Dross formation at the strip exit region

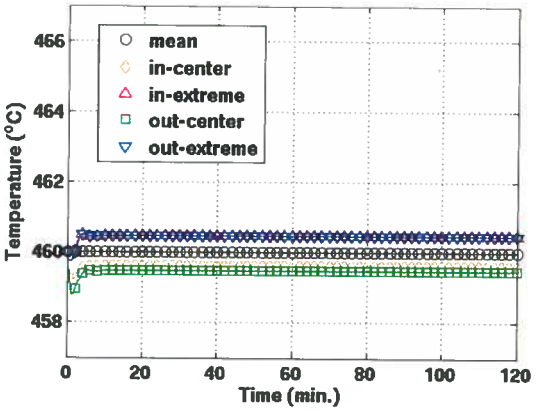

c) Temperature at the snout region

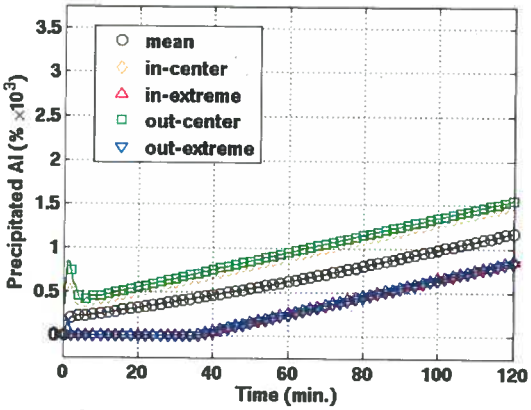

f) Dross formation at the snout region

Figure 5: Local temperature and dross formation characteristics at $\mathbf{T_{strip} = 460°C}$

Dross formation profile

The overall dross formation characteristics of the bath are shown in Figure 4f-j. The regions of the bath where the dross formation rate is higher than the mean value of the bath are shown. As expected, high dross formation rates are observed for all cases at the ingot loading area. The direct influences of the strip entry temperatures can be clearly noticed at the snout and sink roll areas. This is more apparent for the two extreme strip entry temperatures at $T_{strip} = 420°C$ and at $T_{strip} = 500°C$. Besides, the region above the ingot loading area also shows considerable variation in the dross formation. At $T_{strip} = 420°C$, there is very low dross formation at this area. It gradually increases as the strip entry temperature increases.

The local dross formation characteristics at the ingot, the strip exit and the snout regions are shown in Figure 5d-f for the reference case of $T_{strip} = 460°C$. Overall, all local dross formations constantly increase with time. Higher dross formation generally appears at locations with lower local temperatures. There are locations where there is no dross formation at the beginning (e.g. the *up-center* at

the ingot region in Figure 5d). These locations correspond to the areas with higher temperatures, which provide higher Fe solubility limits. Consequently, the formation of dross is delayed until the solute concentration becomes higher.

Similar to the reference case of $T_{strip} = 460°C$, the dross formations constantly increase for both $T_{strip} = 420°C$ (Figure 6d-f), and $T_{strip} = 500°C$ (Figure 7d-f). The parallel relationships between the dross formation and the local temperature can be again observed at these two strip entry temperatures. Wherever the local temperature is low, the dross formation rate becomes high. At $T_{strip} = 420°C$, high dross formation regions include the upper center area at the snout region and the strip exit, as well as the area below the ingot loading region; whereas at $T_{strip} = 500°C$, the high dross formation region includes the *out-center* of the snout region, for example. Note however that the overall dross formation at $T_{strip} = 500°C$ is much lower than that at $T_{strip} = 420°C$.

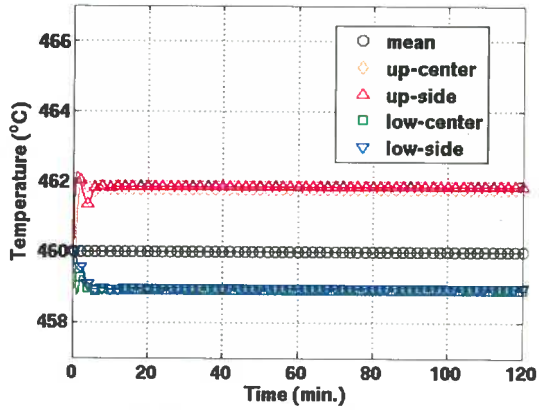

a) Temperature at the ingot region

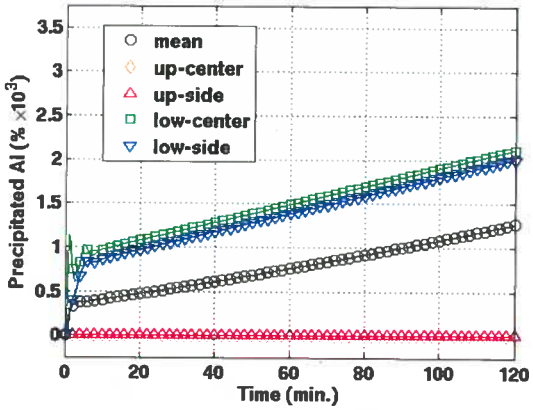

d) Dross formation at the ingot region

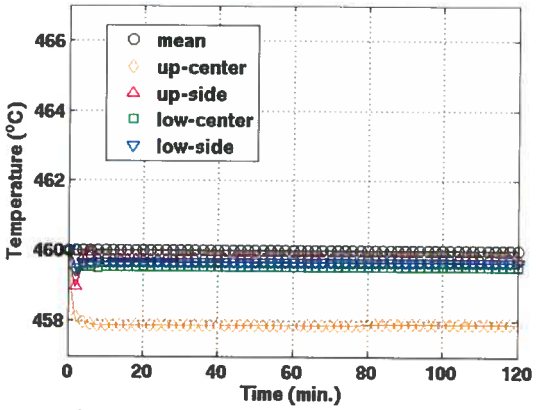

b) Temperature at the strip exit region

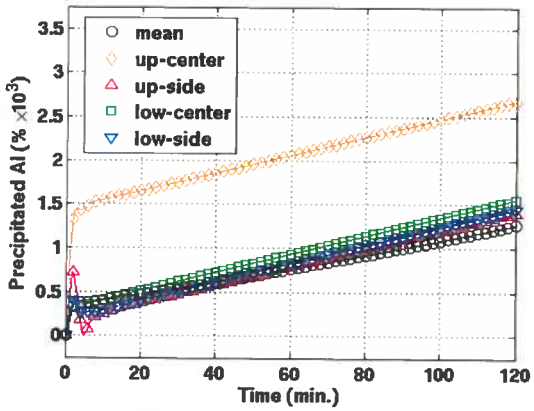

e) Dross formation at the strip exit region

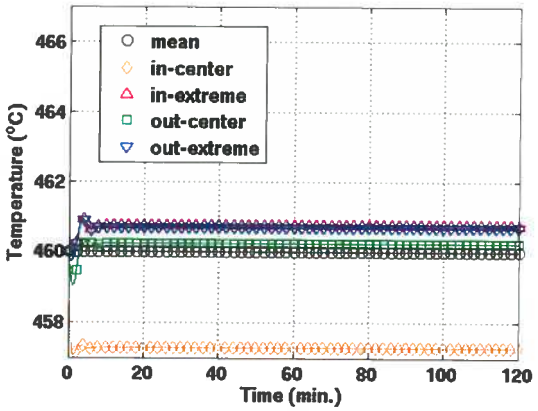

c) Temperature at the snout region

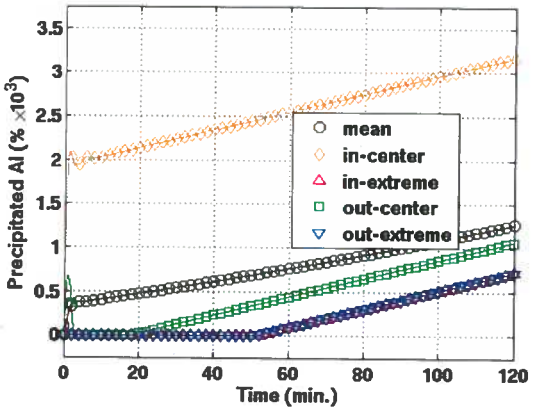

f) Dross formation at the snout region

Figure 6: Local temperature and dross formation characteristics at $T_{strip} = 420°C$

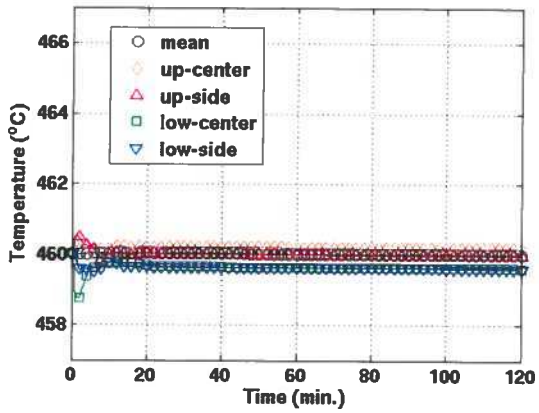

a) Temperature at the ingot region

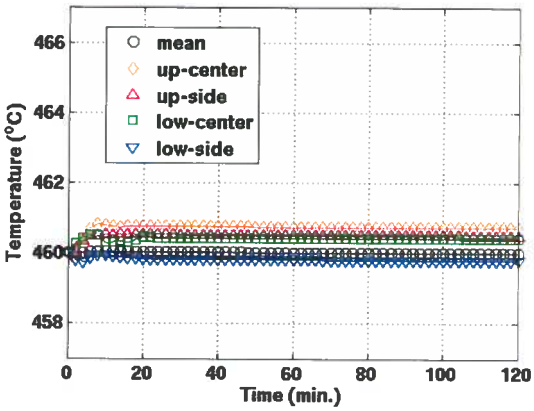

b) Temperature at the strip exit region

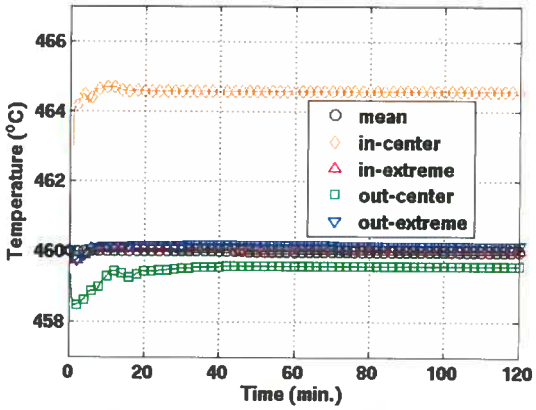

c) Temperature at the snout region

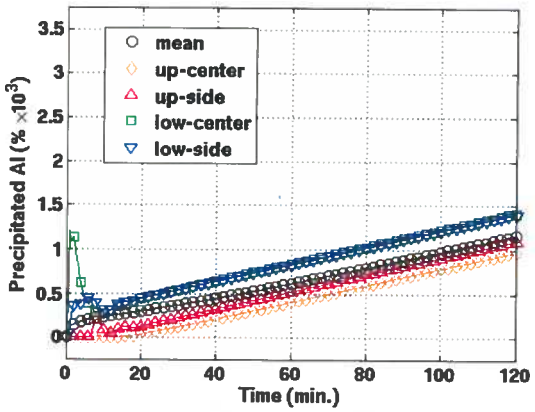

d) Dross formation at the ingot region

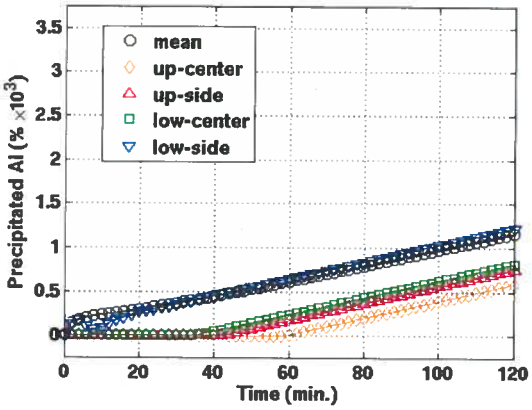

e) Dross formation at the strip exit

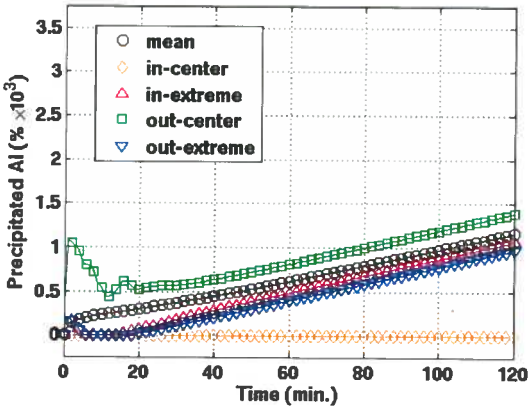

f) Dross formation at the snout region

Figure 7: Local temperature and dross formation characteristics at $\mathbf{T_{strip} = 500°C}$

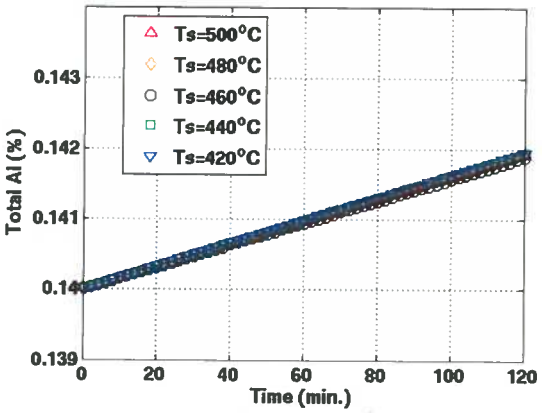

a) Aluminum concentration

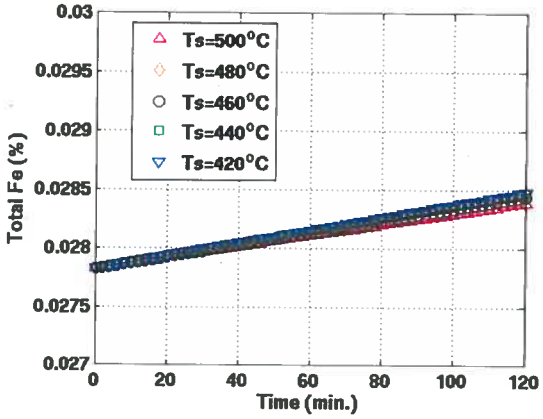

b) Iron concentration

Figure 8: Evolution of overall aluminum and iron concentration

The overall average mean dross formation rates are listed in **Error! Reference source not found.**. The overall dross formation rate is found to decrease as the strip entry temperature increases.

Table 3: Average dross generation rate at different strip entry temperatures

T_{strip}(°C)	Bath average dross	
	kg	wt %
420	7.20	2.97e-3
440	7.01	2.89e-3
460	**6.75**	**2.78e-3**
480	6.68	2.76e-3
500	6.50	2.68e-3

DISCUSSION

The results underline that the strip entry temperature has a strong influence to the galvanizing bath temperature profile. Even though the inductor operation for each case has been adjusted to attain the same overall mean galvanizing bath temperature, the different strip entry temperatures still lead to sufficiently different local temperature fields. Besides, the different strip entry temperatures also induce different rates of iron dissolution and aluminum uptake rates. The combination of these two effects results in considerable differences in the dross formation characteristics.

In particular, it is found that a higher strip entry temperature has a lower global dross production rate. From the perspective of galvanizing bath management, such arrangement seems to be beneficial. Furthermore, based on the initial power consumption analysis, a higher strip entry temperature also consumes less power, being another advantage. Whether a higher strip temperature would be a feasible mean to reduce dross in production certainly depends on many more factors. For example, the microstructure of the substrate will need to be stable enough for the cases with increased strip temperature.

Noting the importance of local temperature profile for dross formation, it will be worthwhile to determine if it will be more advantageous to operate the inductor using a high temperature-low flow arrangement as compared to the high flow-low temperature arrangement considered here. Numerical simulations are underway, and the results will be reported in the future.

CONCLUSIONS

In the present study, the effect of the strip entry temperature on galvanizing bath management is examined numerically using a well-validated galvanizing bath model. The impacts are quantified in terms of the bath flow, temperature and compositional characteristics, as well as the dross formation pattern for five different strip entry temperatures from 420 to 500°C. For each case, the Fe dissolution and Al uptake rates are adjusted according to the predictions of the MAP (Modeling Aluminum Pick-up) program from Teck Metals Ltd. It is found that the difference in the strip entry temperature can induce substantial variations in the galvanizing bath temperature field. The results of the present study suggest that a higher strip entry temperature may be potentially beneficial to reduce both the power consumption and the overall dross formation. Certainly, it demands a good local temperature management to prevent excessive dross formation.

ACKNOWLEGEMENT

The authors would like to thank Dr. Daniel Liu from Teck Metals Ltd. for the insightful discussions and providing the strip Fe dissolution and Al uptake data. The authors would also like to acknowledge the International Zinc Association, the sponsors of the Galvanized Autobody Partnership program ZCO-71 and the Advanced Manufacturing and Design Systems program of NRC for making this work possible.

REFERENCES

[1] S. Keeler and M. Kimchi, Eds., "Advanced High Strength Steel (AHSS) Application Guidelines." World Steel Association, 2014.

[2] F. Ajersch, M. Gauthier, and C. Binet, "Kinetics of continuous galvanizing process," in *Fundamentals of metallurgical processing: proceedings of James M. Toguri Symposium - MetSoc 39th Annual Conference of Metallurgists of CIM, August 20 - 23, 2000, Ottawa, Ontario, Canada*, G. Kaiura, C. Pickles, T. Utigard, and A. Vahed, Eds. Montreal: Canad. Inst. of Mining, Metallurgy and Petroleum, 2000, pp. 161–178.

[3] F. Ilinca, J.-F. Hétu, and F. Ajersch, "Three-dimensional numerical simulation of turbulent flow and heat transfer in a continuous galvanizing bath," *Numer. Heat Transf. Part Appl.*, vol. 44, no. 5, pp. 463–482, 2003.

[4] F. Ajersch, F. Ilinca, and J.-F. Hétu, "Simulation of Flow in a Continuous Galvanizing Bath: Part I. Thermal Effects of Ingot Addition," *Metall. Mater. Trans. B Process Metall. Mater. Process. Sci.*, vol. 35, no. 1, pp. 161–170, 2004.

[5] F. Ajersch, F. Ilinca, and J.-F. Hétu, "Simulation of Flow in a Continuous Galvanizing Bath: Part II. Transient Aluminum Distribution Resulting from Ingot Addition," *Metall. Mater. Trans. B Process Metall. Mater. Process. Sci.*, vol. 35, no. 1, pp. 171–178, 2004.

[6] F. Ajersch, F. Ilinca, and F. E. Goodwin, "Numerical simulation of flow, temperature and composition variation in the snout and sink roll region of continuous galvanizing baths," in *Materials Science and Technology Conference and Exhibition 2013, MS and T 2013*, 2013, vol. 2, pp. 1145–1152.

[7] F. Ilinca, F. Ajersch, C. Baril, and F. E. Goodwin, "Numerical simulation of the galvanizing process during GA to GI transition," *Int. J. Numer. Methods Fluids*, vol. 53, no. 10, pp. 1629–1646, 2007.

[8] A. R. Marder, "Metallurgy of zinc-coated steel," *Prog. Mater. Sci.*, vol. 45, no. 3, pp. 191–271, 2000.

[9] F. Ilinca and D. Pelletier, "Positivity preservation and adaptive solution for the k-∈ model of turbulence," *AIAA J.*, vol. 36, no. 1, pp. 44–50, 1998.

[10] N.-Y. Tang, "Refined 450°C isotherm of Zn-Fe-Al phase diagram," *Mater. Sci. Technol.*, vol. 11, no. 9, pp. 870–873, 1995.

[11] N.-Y. Tang, "Determination of liquid-phase boundaries in Zn-Fe-Mx systems," *J. Phase Equilibria*, vol. 21, no. 1, pp. 70–77, 2000.

[12] L. P. Franca and S. L. Frey, "Stabilized finite element methods: II. The incompressible Navier-Stokes equations," *Comput. Methods Appl. Mech. Eng.*, vol. 99, no. 2–3, pp. 209–233, 1992.

[13] Y. H. Liu and N.-Y. Tang, "Computer modeling of aluminium uptake and iron dissolution in galvanizing and galvannealing," in *Galvatech '04: 6th International Conference on Zinc and Zinc Alloy Coated Steel Sheet - Conference Proceedings*, 2004, pp. 1155–1164.

[14] Y. H. Liu, "Experimental Validation of Computer Simulation of Aluminum Pickup and Iron Dissolution in Galvanneal and Galvanize Production," in *Galvatech 2015 Proceedings*, 2015, pp. 545–552.

[15] M. Dutta and S. B. Singh, "Effect of strip temperature on the formation of an Fe2Al5 inhibition layer during hot-dip galvanizing," *Scr. Mater.*, vol. 60, no. 8, pp. 643–646, 2009.